Preprint

Experimental study of smear formation and removal in heat-assisted magnetic recording

Qilong Cheng, David B. Bogy
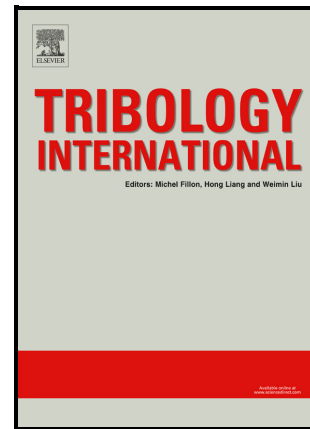
Experimental study of smear formation and removal in heat-assisted magnetic recording

Qilong Cheng[1, a)] and David B. Bogy[1]

University of California at Berkeley, Berkeley, California 94720,

USA.

The head-disk interface (HDI) in heat-assisted magnetic recording (HAMR) hard disk drives is a system where a laser beam is launched from a recording head and focused on a recording disk to facilitate data writing. During the laser exposure, material transfers from the disk to the head surface due to the high temperature field and steep thermal gradient. The material accumulation on the head surface, also known as smear, is a challenging reliability issue for HAMR. In this paper, we experimentally investigated the effect of disk temperature and laser exposure time on the smear formation and studied the smear removal by frictional interactions between the head and the disk. In the experiments, the disk temperature and the laser exposure time were controlled separately to generate the smear, which was later characterized by atomic force microscopy (AFM). The AFM images show that the smear forms when the lubricant evaporation occurs for a certain time, and that the smear amount increases with the disk temperature and the laser exposure time. Furthermore, touchdown experiments were performed using the heads with smear. The results indicate that the smear is mostly removed by friction from the head-disk contact. This study reveals the mechanism of the smear formation in HAMR and presents a mechanical approach to mitigate the smear without damaging the head.

Keywords: heat-assisted magnetic recording (HAMR); head-disk interface (HDI); laser; smear; friction

---

[a)]Email: qlcheng@berkeley.edu

I. INTRODUCTION

As one of the most promising technologies to boost the areal density of hard disk drives over 3 Tb/in^2, heat-assisted magnetic recording (HAMR) has been studied extensively and is approaching commercialization[1,2]. Such high areal densities require high-coercivity magnetic disks for data stability. Compared with conventional perpendicular magnetic recording (PMR), the HAMR technology contains additional components such as a laser diode, a waveguide (WG), a near field transducer (NFT) in the recording head and a heatsink in the recording disk[3,4]. As shown in Figure 1, a laser beam is launched from the recording head and is focused on the recording disk to locally heat the disk to its Curie temperature (400-500 °C)[1,5]. Thus, the coercivity of the magnetic layer in the disk is lowered and data writing can be performed. Therefore, the head-disk interface (HDI) of HAMR is a tribology system that combines nanoscale spacing (< 15 nm), high temperature, steep thermal gradient, and high-speed sliding condition (5-40 m/s)[1,6]. The HDI performance directly determines the lifetime of the HAMR product[6,7].
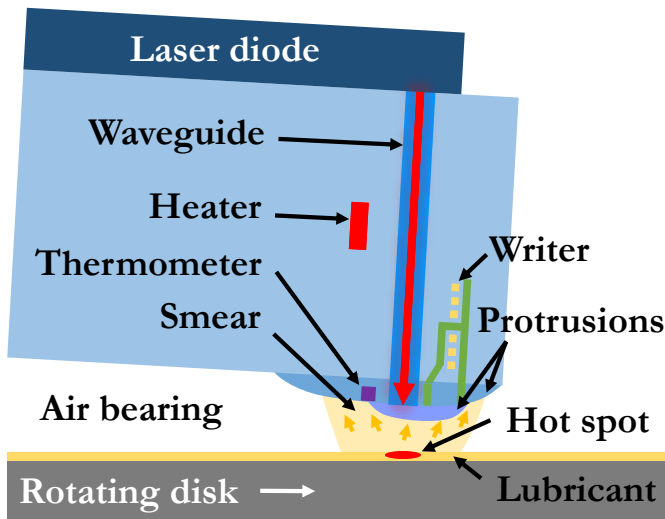
FIG. 1. A schematic diagram of the HAMR head-disk interface (not to scale).

During the laser exposure, mass transfer also happens due to the high level of heat transfer in the HAMR HDI. The temperature of the hot spot (400-500 °C) is much higher than the lubricant evaporation temperature (150-250 °C) under HAMR operations[8,9], so the lubricant is evaporated from the disk and then condenses on the head surface. The material

Cheng et al.

accumulation on the head surface, also known as smear, is a challenging reliability issue for HAMR[6,10]. The smear could affect the head's flyability as well as the heat transfer and the NFT efficiency of laser delivery in the HAMR head-disk interface, which may finally lead to the device failure[10–14].

In previous studies, Raman *et al.*[11] reported flyability failures due to contamination at the head-disk interface using a full body capacitance method. Their experiments showed that the contamination could affect the flying height and result in a crash of the head-disk interface. Yang *et al.*[12] studied the lubricant transfer and deposition from the disk to the head during HAMR writing, which was attributed to a temperature difference inversion at the head-disk interface. Xiong *et al.*[13] found that the material accumulation on the head surface could be deposited back to the disk, where mechanical interaction plays an important role. Kiely *et al.*[10] investigated the driving forces, growth mechanisms, and growth rates of head contamination, and they proposed an evaporation-condensation model. They demonstrated that the head may be overheated and the NFT efficiency may be affected due to the presence of the contamination, which depends on the contamination properties.

In this paper, we performed HAMR-writing experiments and touchdown experiments to generate/remove the smear for understanding the smear formation and its mitigation. When generating the smear, we controlled laser current (disk temperature) and laser exposure time separately to investigate their effects. The smear that formed on the head surface was later characterized by atomic force microscopy (AFM). Furthermore, repeated touchdowns were performed using heads with the smear to study the smear removal. This study reveals the mechanism of the smear formation in HAMR and presents a mechanical approach to removal of the smear without damaging the head, which are important to the HAMR hard disk drive's performance and reliability.

II.   EXPERIMENTAL SETUP

The experiments were conducted using a component-level HAMR test stage as shown in Figure 2. A HAMR head (without NFT) flies above a rotating HAMR disk (5400 rpm) with a relative speed $\sim$ 15 m/s. The elements in the head, including a heater, writer, laser and thermometer, were controlled by a data acquisition toolbox. The heater was energized to create a local protrusion at the head surface, thus bringing it towards the disk. The

3
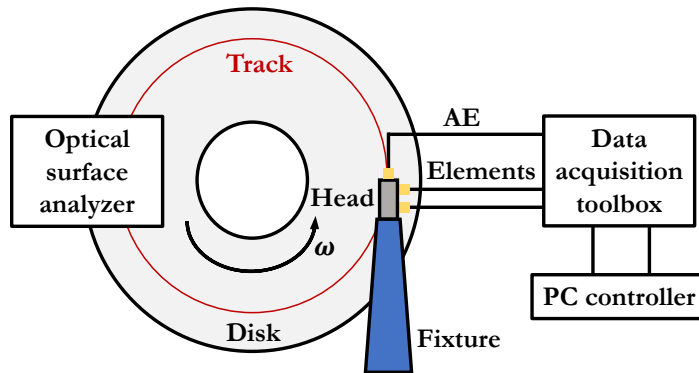
FIG. 2. A schematic diagram of the experimental setup.

clearance between the head and the disk was adjusted by changing the heater power[15–17]. During the HAMR-writing experiments to generate the smear, the heater power was kept at the touchdown power (TDP) minus 80 mW to maintain a head-disk clearance $\sim$ 5-6 nm, where the TDP denotes the heater power when the heater protrusion comes into contact with the disk. The writer was biased at -65 mA using a DC current source. The laser current was increased to calibrate the disk temperature. Then, the effects of the disk temperature and the laser exposure time on the smear formation were investigated. A thermometer embedded near the head surface (see Figure 1) was used to measure the head temperature[18–20], and an acoustic emission (AE) sensor was mounted on the head fixture to monitor the head-disk contact[21]. The stationary head flies on a single track with the track width $\sim$ 300 nm. Above the other half of the rotating disk, an optical surface analyzer (OSA, Candela 5100) was used to in-situ characterize the lubricant uniformity in the track. Thereafter, the touchdown experiments for the smear removal were performed using the heads with the smear. The heater power was ramped up until TDP+2 mW, and the head temperature was measured

TABLE I. Experimental parameters

Elements	Smear generation	Smear removal
Heater	TDP-80 mW	0-TDP+2 mW
Writer	-65 mA DC	OFF
Laser	ON, 0-40.8 mA DC	OFF
Thermometer	ON, 1 mA DC	ON, 1 mA DC

using the thermometer. The laser and the writer were OFF during the touchdowns. The details of the experimental parameters can be found in Table I.

III. RESULTS AND DISCUSSION

A. Effect of disk temperature
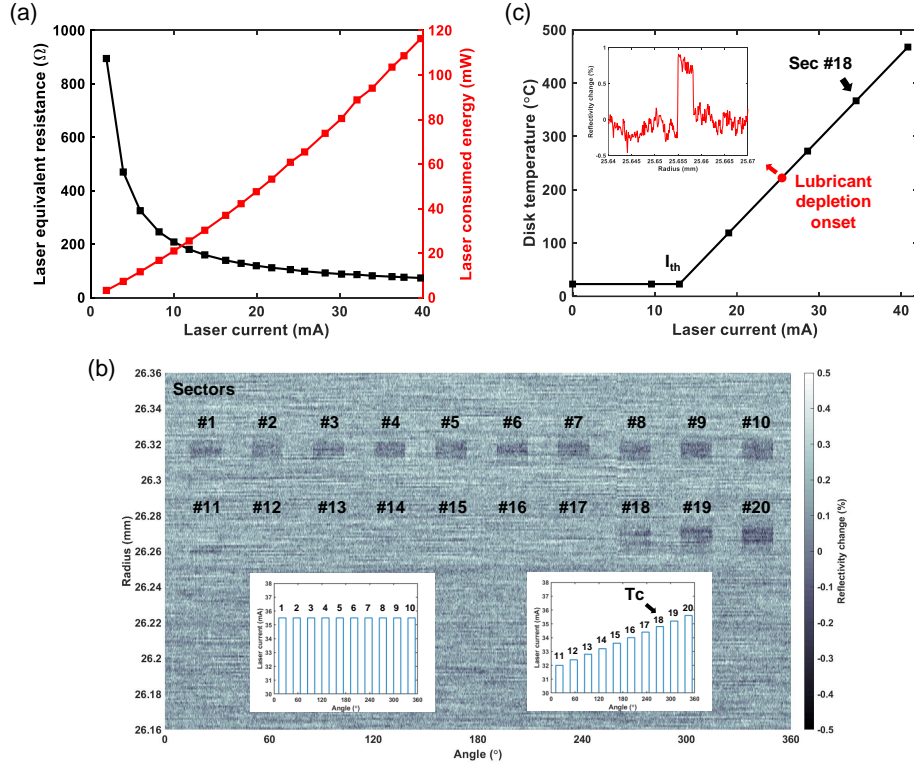
FIG. 3. Disk temperature calibration. (a) Laser equivalent resistance and laser consumed energy as a function of the laser current. (b) A magnetic image of 20 sectors under HAMR writing with different laser currents. Inset: the laser currents for the sectors. (c) Main: calibrated disk temperature. Inset: reflectivity change of the band at the lubricant depletion onset.

In this section, we study the effect of the disk temperature on the smear formation. The disk temperature is dependent on the laser current. Figure 3 shows the calibration experiments for the disk temperature. In Figure 3(a), the laser equivalent resistance and the laser consumed energy are plotted as a function of the laser current. The curves show that the laser equivalent resistance decreases with the laser current and finally levels off to $\sim 80\ \Omega$. The laser consumed energy generally presents a linear relation with the laser current, which

Cheng et al.

is used in the following calibration for the disk temperature. Figure 3(b) shows an OSA magnetic image of 20 sectors under HAMR writing with write current -65 mA and different laser currents, where sectors #1-#10 are location markers with a constant laser current (high enough to write), and sectors #11-#20 are the ones with increasing laser currents. Here, the head was moved radially by ~ 10 μm to create a uniform band, due to the fact that the laser spot size is ~ 300 nm which is much smaller than the OSA's resolution in micrometers. It is observed that the writing effect does not appear until sector #18, indicating that the sector #18 is the writing onset, and its disk temperature corresponds to the magnetic layer's writing-onset temperature ~ 367.0 °C[22] during the HAMR operations. Also, the laser diode has a threshold of 13.0 mA, below which no light emits. Since the laser consumed energy has an approximately linear relation with the laser current, the disk temperature rise due to the laser heating is also assumed to be linear with the laser current. Then, linear interpolation and extrapolation are performed for the disk temperature calibration using the threshold datapoint (13.0 mA, 23 °C) and the writing-onset datapoint (34.5 mA, 367.0 °C) as plotted in Figure 3(c). As the laser current ramps up, the OSA was used to monitor the lubricant uniformity under the laser exposure. Figure 3(c) inset shows the reflectivity change at the lubricant depletion onset with the disk temperature of ~ 220 °C. The positive peak in Figure 3(c) implies that the lubricant within the band is depleted during the laser exposure, and that the lubricant has an evaporation temperature ~ 220 °C.
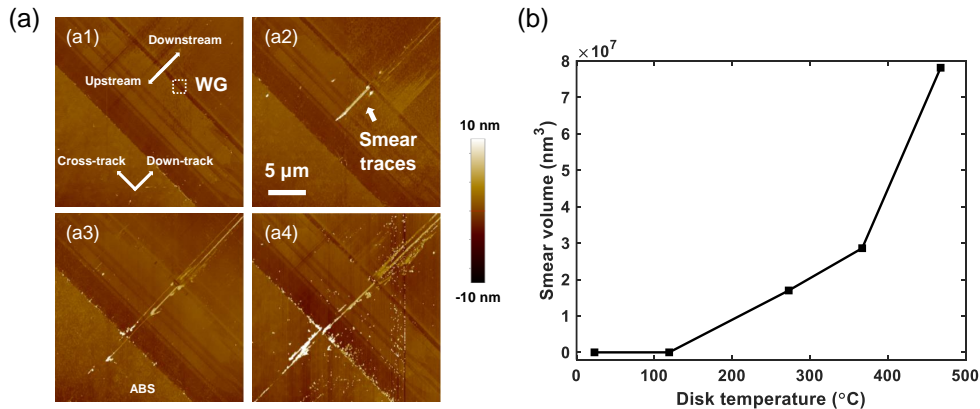
FIG. 4. Effect of disk temperature on smear. (a) AFM images of the smear at the disk temperature (a1) 119.0 °C (a2) 272.6 °C (a3) 367.0 °C (a4) 467.8 °C with a constant laser exposure time of 111.1 s. (b) Smear volume as a function of the disk temperature.

6

Cheng et al.

With the disk temperature calibrated using the writing-onset temperature, we then studied its effect on the smear formation. Figure 4(a) shows the AFM images of the smear at different disk temperatures (a1) 119.0 °C (a2) 272.6 °C (a3) 367.0 °C (a4) 467.8 °C with a constant laser exposure time of 111.1 s (10^4 revolutions). The AFM images were scanned at scan angle 45 degrees to avoid imaging artifacts. The cross-track and down-track directions are denoted in Figure 4(a1). The relative sliding speed between the head and the disk was along the down-track direction with a zero skew angle. In Figure 4(a1), no smear appears because the disk temperature 119.0 °C is much lower than the lubricant evaporation temperature ~ 220 °C. For higher disk temperatures (272.6-467.8 °C), the smear forms in the shape of traces as shown in Figures 4(a2-a4). Figure 4(a2) shows that the smear traces originate from the WG location and form along the down-track direction, in both the downstream and upstream paths. The disk rotates towards the downstream down-track direction, so the air flow carries the lubricant evaporation generated near the WG location to the downstream head surface, and thus the lubricant condenses there as the smear. The smear also forms upstream from the WG location, which is caused by the mechanical interaction between the head and the disk[10,13]. The smear fills the head-disk gap and then materials on the disk are picked up and transferred from the disk to the upstream head surface by mechanical contact, as illustrated in Figure 1. Figures 4(a3-a4) show that the smear evolves upstream as far as the AlTiC air bearing surface (ABS). Also, the AFM images show that the smear is primarily located along the two down-track sides of the WG (~ 350 nm from the center), which may be because the thermocapillary stress dominates and pushes the condensed lubricant away from the down-track central line[23]. Furthermore, particulate-like smear is observed in Figure 4(a4), which comes from the magnetic layer[24], indicating that the lubricant and carbon protective layer may be depleted completely and the magnetic layer is damaged under such a high temperature 467.8 °C. Figure 4(b) plots the generated smear volume as a function of the disk temperature. The smear is generated when the disk temperature is higher than the lubricant evaporation temperature (~ 220 °C), and its amount increases nonlinearly with the disk temperature.

B.   Effect of laser exposure time

Next we investigate the effect of the laser exposure time on the smear formation. Figure 5(a) shows the AFM images of the smear at different laser exposure times (a1) 1.1 s (a2) 11.1 s (a3) 111.1 s (a4) 1111.1 s with a constant disk temperature of 367.0 °C (writing-onset temperature). The disk temperature is higher than the lubricant evaporation temperature, but there is no smear present in Figure 5(a1), which indicates that the laser exposure time 1.1 s is too short for the lubricant evaporation to reach the head surface and condense. At the laser exposure time 11.1 s, Figure 5(a2) shows a small smear dot exactly at the WG location, which is assumed to be the onset of the smear formation. Then, the smear dot evolves into traces over time which extend to the AlTiC ABS as well, as shown in Figures 5(a3-a4). Figure 5(b) plots the smear volume as a function of the laser exposure time. When the disk temperature is higher than the lubricant evaporation temperature, it takes a certain time (a value between 1.1 s and 11.1 s) for the smear to form on the head surface. Thereafter, the smear amount increases with the laser exposure time.

To better understand the smear formation, Figures 5(c-d) show the height profiles of the smear on the head surface along the down-track direction. Figure 5(d) shows the zoom-in height profiles of Figure 5(c) near the WG location. In Figure 5(c), the locations of the ABS, the heater protrusion and the WG are marked in the down-track position. For the laser exposure time 1.1 s, no smear appears in Figures 5(c-d), so the blue curve is the height profile of the head surface without any smear. When the laser exposure time is 11.1 s, a smear dot of $\sim$ 2 nm high shows up at the WG location in Figure 5(d), which is the smear formation onset. For the cases of longer laser exposure times 111.1 s and 1111.1 s, Figure 5(c) shows that the smear forms both downstream (positive x axis) and upstream (negative x axis). In the downstream direction, the yellow curve (111.1 s) shows some discrete smear, while the purple curve (1111.1 s) presents a continuous smear trace, indicating that the smear accumulates over time. The smear is also observed at the heater protrusion location. During the HAMR-writing experiments to generate the smear, the physical clearance between the heater protrusion and the disk was kept $\sim$ 5-6 nm, so the smear height cannot exceed this value. In Figure 5(c), the smear height near the heater protrusion location is exactly $\sim$ 5-6 nm, which implies that the smear grows and fills the head-disk gap. Moreover, several smear dots are seen at the ABS location and their heights

8

Cheng et al.
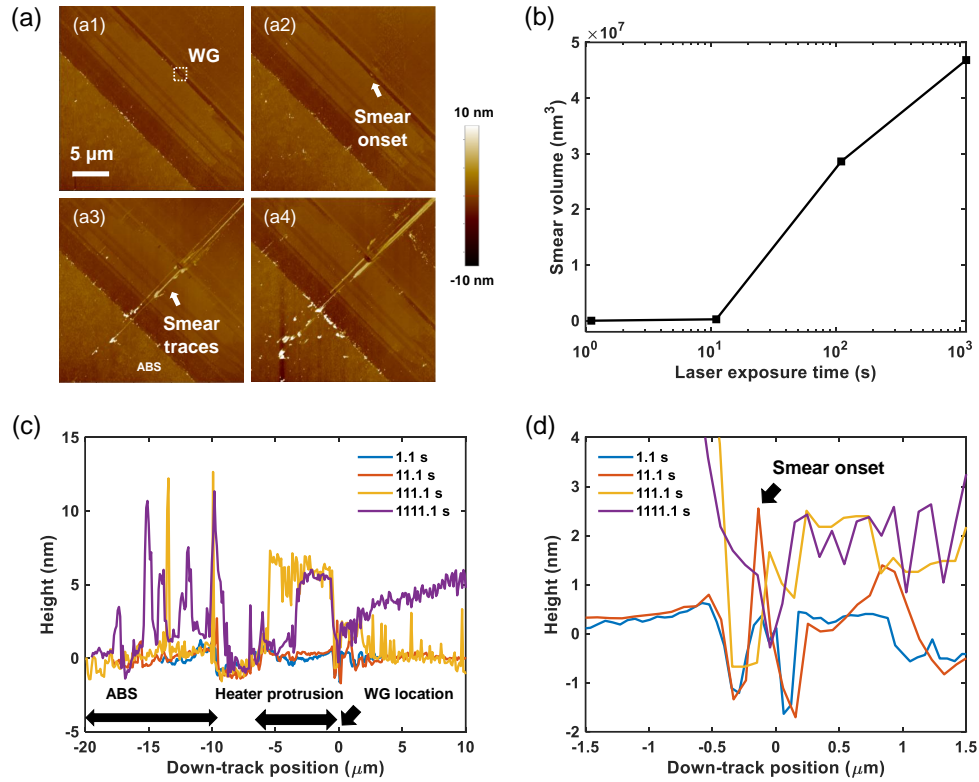
FIG. 5. Effect of laser exposure time on smear. (a) AFM images of the smear at the laser exposure time (a1) 1.1 s (a2) 11.1 s (a3) 111.1 s (a4) 1111.1 s with a constant disk temperature of 367.0 °C. (b) Smear volume as a function of the laser exposure time. (c) Height profiles of the smear along the down-track direction and (d) their zoom-in near the WG location.

have a maximum value ~ 12 nm, which is related to the initial head-disk clearance ~ 10-15 nm. There is no protrusion bulging on the AlTiC ABS, so the smear height on the ABS is limited by the initial clearance. With the head-disk interface filled with the smear at the heater protrusion location, the mechanical contact drives the materials on the disk to the head surface upstream, forming the smear dots on the ABS. In summary, the height profiles in Figures 5(c-d) verify that the smear can fill the head-disk interface gradually, and later grow upstream to the ABS, which is caused by the mechanical interaction between the smear on the head surface and the rotating disk.

Cheng et al.

C. Smear removal by friction

In this section, the smear removal is studied by use of touchdown experiments. During the touchdowns, the heater power was increased beyond the touchdown power (TDP+2 mW) where the AE sensor starts to detect the head-disk contact. Thus, the heater protrusion fills the head-disk gap and gets into contact with the surface of the rotating disk. It is noted that the writer and the laser are OFF here. Specifically, 10 repeated touchdowns were performed using a head that already had some smear on its surface. Figure 6(a) shows the AFM images of the head surface with smear and after 10 repeated touchdowns. Clearly, the smear present in Figure 6(a1) is mostly gone after the touchdowns, except for some particles which are not positioned at the heater protrusion location. The head surface remains intact after such a slight touchdown process, and the head also remains functional. The comparison demonstrates that the friction induced by the contact between the head protrusion and the disk removes the smear effectively without damaging the head.
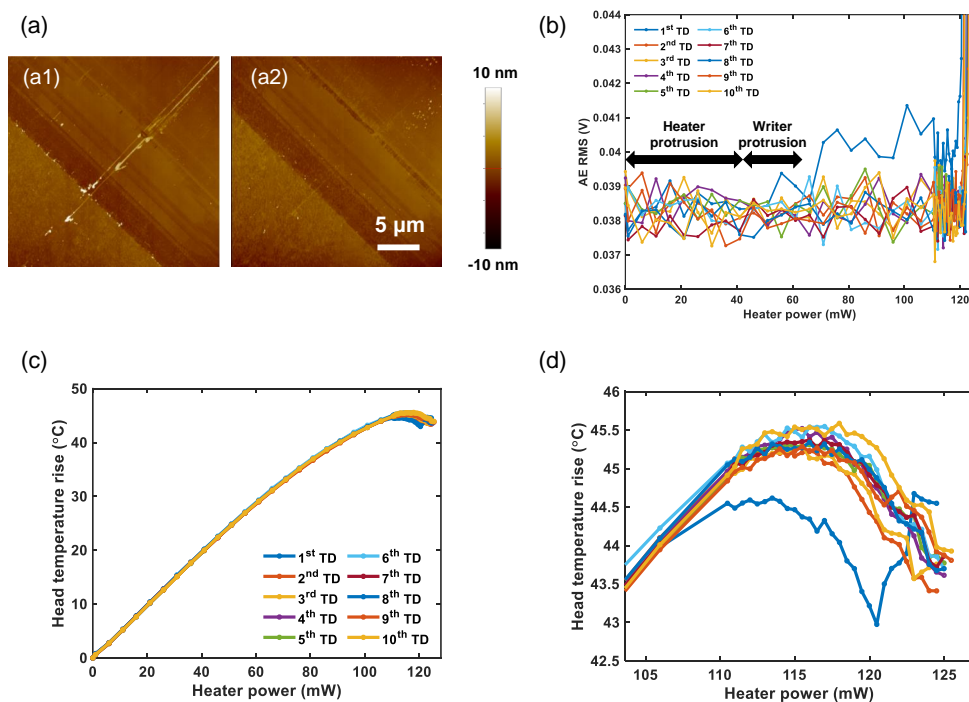
FIG. 6. Effect of touchdowns (TDs) on smear. (a) AFM images of the head surface (a1) with smear and (a2) after 10 repeated touchdowns. (b) AE RMS signal as a function of the heater power during the touchdowns. (c) Head temperature rise as a function of the heater power during the touchdowns and (d) its zoom-in near contact.

Cheng et al.

Figure 6(b) and Figure 6(c) show the the root mean square (RMS) of the AE signal and the head temperature rise as a function of the heater power during the 10 touchdowns, respectively. For each data point, the heater power was maintained for 0.11 s (10 revolutions) to obtain the AE RMS signal and the average temperature rise. Interestingly, Figure 6(b) shows that the 1st touchdown curve differs from the other curves (2nd-10th touchdowns) in that it has some AE signal higher than the baseline value ($\sim$ 0.039 V) at the heater power between 66 mW and 120 mW. This unusual signal during the 1st touchdown is caused by the smear removal. The heater power 0-120 mW (TDP) in Figure 6(b) corresponds to the gap between the head surface (without any protrusion) and the disk surface. During the smear generation experiment for the head shown in Figure 6(a1), the heater power was 42 mW and the writer was energized with its protrusion equivalent to $\sim$ 20 mW heater power change, so the heater protrusion and the writer protrusion correspond to the regions 0-42 mW and 42-62 mW as denoted in Figure 6(b). The laser-induced protrusion is neglected here because it is only several angstroms[25]. The smear filled the gap between the head protrusion (heater protrusion + writer protrusion, 0-62 mW) and the disk, and thus could only occupy the region 62-120 mW, which is exactly where the unusual AE signal appears. This indicates that the smear was removed by the frictional interactions from the head-disk contact, which produced vibrations and was detected by the AE sensor. Moreover, this AE signal that appears in the region 62-120 mW vanishes from the 2nd touchdown to the 10th touchdown, implying that the smear was primarily burnished away during the 1st touchdown and that there is no smear effect thereafter.

The head temperature measurement shows a similar feature that the 1st touchdown curve is different from the other ones. Figure 6(c) and its zoom-in Figure 6(d) show that the head temperature rise is lower ($\sim$ 2 °C) during the 1st touchdown and gets back to normal from the 2nd touchdown, indicating that the smear removal leads to more heat transfer before the real touchdown that occurs at 120 mW. The smear may form a material bridge at the head-disk interface and transfers the heat across it, lowering the head temperature. And the smear is primarily removed during the 1st touchdown, so the frictional heating is expected be negligible as the smear is burnished away.

11

Cheng et al.

IV. CONCLUSIONS

In conclusion, we performed HAMR-writing experiments and touchdown experiments to investigate the smear formation and removal. The experimental results show that the smear begins to form when the disk temperature is higher than the lubricant evaporation temperature, and the evaporation occurs for a certain time, which is long enough for the lubricant evaporation to reach the head surface and condense. The smear originates from the WG location and forms into traces along the down-track direction. The smear traces are primarily located at a distance from the track center, which is likely due to the thermocapillary stress. Particulate-like smear that comes from the magnetic layer appears at a higher disk temperature. And the smear amount increases with the disk temperature and the laser exposure time. Moreover, it is demonstrated that the mechanical interactions of touchdown can be used to mitigate the smear. The smear is removed by the friction from the head-disk contact during touchdowns without damaging the head. Meanwhile, the burnishing away of the smear is detected by the AE sensor, and this leads to more heat transfer at the head-disk interface, thereby lowering the head temperature by $\sim 2\,°\mathrm{C}$. It is envisioned that the insights obtained from this study on the smear will be important to the HAMR hard disk drive's performance and reliability.

REFERENCES

[1] M. H. Kryder, E. C. Gage, T. W. McDaniel, W. A. Challener, R. E. Rottmayer, G. Ju, Y.-T. Hsia, and M. F. Erden, Proceedings of the IEEE **96**, 1810 (2008).

[2] W. Challener, C. Peng, A. Itagi, D. Karns, W. Peng, Y. Peng, X. Yang, X. Zhu, N. Gokemeijer, Y.-T. Hsia, *et al.*, Nature photonics **3**, 220 (2009).

[3]L. Pan and D. B. Bogy, Nature Photonics **3**, 189 (2009).

[4]B. C. Stipe, T. C. Strand, C. C. Poon, H. Balamane, T. D. Boone, J. A. Katine, J.-L. Li, V. Rawat, H. Nemoto, A. Hirotsune, *et al.*, Nature photonics **4**, 484 (2010).

[5]E. Schreck, D. Li, S. V. Canchi, L. Huang, G. P. Singh, B. Marchon, H. J. Richter, B. Stipe, and M. Staffaroni, IEEE transactions on magnetics **50**, 126 (2014).

[6]J. D. Kiely, P. M. Jones, and J. Hoehn, MRS Bulletin **43**, 119 (2018).

[7]B. Marchon, T. Pitchford, Y.-T. Hsia, and S. Gangopadhyay, Advances in Tribology **2013** (2013).

[8]M. S. Lim and A. J. Gellman, Tribology international **38**, 554 (2005).

[9]N. Tagawa and H. Tani, IEEE transactions on magnetics **47**, 105 (2010).

[10]J. D. Kiely, P. M. Jones, Y. Yang, J. L. Brand, M. Anaya-Dufresne, P. C. Fletcher, F. Zavaliche, Y. Toivola, J. C. Duda, and M. T. Johnson, IEEE Transactions on Magnetics **53**, 1 (2016).

[11]V. Raman, D. Gillis, and R. Wolter, J. Trib. **122**, 444 (2000).

[12]Y. Yang, X. Li, M. Stirniman, X. Yan, F. Huang, F. Zavaliche, H. Wang, J. Huang, H. Tang, P. M. Jones, *et al.*, IEEE Transactions on Magnetics **51**, 1 (2015).

[13]S. Xiong, N. Wang, R. Smith, D. Li, E. Schreck, and Q. Dai, Tribology Letters **65**, 74 (2017).

[14]J. Aoyama, M. Furukawa, S. Nishida, K. Tasaka, K. Matsuda, K. Kuroki, and M. Ikeda, IEEE Transactions on Magnetics **53**, 1 (2017).

[15]Y. Ma, A. Ghafari, B. Budaev, and D. Bogy, Applied Physics Letters **108**, 213105 (2016).

[16]Q. Cheng, S. Sakhalkar, A. Ghafari, Y. Ma, and D. Bogy, Applied Physics Letters **116**, 213102 (2020).

[17]S. Sakhalkar, Q. Cheng, A. Ghafari, and D. Bogy, Journal of Applied Physics **128**, 084301 (2020).

[18]J. Xu, Y. Shimizu, M. Furukawa, J. Li, Y. Sano, T. Shiramatsu, Y. Aoki, H. Matsumoto, K. Kuroki, and H. Kohira, IEEE transactions on magnetics **50**, 114 (2014).

[19]H. Wu, S. Xiong, S. Canchi, E. Schreck, and D. Bogy, Applied Physics Letters **108**, 093106 (2016).

[20]Q. Cheng, S. Rajauria, E. Schreck, R. Smith, N. Wang, J. Reiner, Q. Dai, and D. Bogy, Scientific reports **10**, 1 (2020).

Cheng et al.

[21]S. Rajauria, O. Ruiz, S. V. Canchi, E. Schreck, and Q. Dai, Physical review letters **120**, 026101 (2018).

[22]A. Chernyshov, T. Le, B. Livshitz, O. Mryasov, C. Miller, R. Acharya, and D. Treves, Journal of Applied Physics **117**, 17D111 (2015).

[23]S. V. Sakhalkar and D. B. Bogy, IEEE Transactions on Magnetics **55**, 1 (2018).

[24]S. Xiong, R. Smith, E. Schreck, and Q. Dai, Tribology Letters **69**, 1 (2021).

[25]Q. Cheng, H. Wang, S. V. Sakhalkar, and D. B. Bogy, Applied Physics Letters **117**, 153105 (2020).